

Numerical analysis of Al_2O_3 /water nanofluid natural convection in a square cavity filled with an anisotropic porous medium under a magnetic field

S. SAFI^{1,2)}, F. BERRAHIL^{2,3)}, A. FILALI^{4,5)}, S. BENISSAAD²⁾

¹⁾ *Department of Climatic Engineering, Faculty of Sciences Technology, University of Constantine 1, Frères Mentouri, Constantine, Algeria, e-mail: safia.safi@umc.edu.dz (corresponding author)*

²⁾ *LEAP Laboratory, Department of Mechanical Engineering, Faculty of Sciences Technology, University of Constantine 1, Frères Mentouri, Constantine, Algeria*

³⁾ *Department of Mechanical and Electromechanical Engineering, Sciences and Technology Institute, University Center Abdelhafid Boussouf, Mila, Algeria*

⁴⁾ *Laboratoire de Mécanique et de systèmes énergétiques avancés, École Nationale Polytechnique de Constantine, Algeria*

⁵⁾ *Chemical Engineering Department, Imperial College London, South Kensington, London SW7 2AZ, UK*

NATURAL CONVECTION IN POROUS MEDIA IS CRUCIAL for applications such as geothermal energy cooling systems and energy storage, where efficient heat transfer is essential. However, the combined effect of anisotropy in the porous matrix and an inclined magnetic field on nanofluid heat transfer remains poorly understood hence, this study addresses numerically the unexplored combined effects of anisotropy and inclined magnetic field on the natural convection of water-based Al_2O_3 nanofluid. The Darcy–Brinkman–Forchheimer model and energy transport equations describe nanofluid motion and heat transfer in a porous medium. The mathematical equations are discretized using the finite volume method in an in-house computer code. The governing parameters are the Rayleigh number the Darcy number, the Hartmann number, solid volume fraction, the permeability ratio K (a measure of porous medium anisotropy) and an inclination angle with the magnetic field. Results are reported for streamlines, temperature contours, and the average Nusselt number under different parametric conditions. It was found that increasing the Rayleigh and Darcy numbers shifts the system from conduction to convection, improving the heat transfer rate. The nanoparticle volume fraction enhances heat transfer in conduction-dominated flows but reduces it in convection-dominated regimes. A higher Hartmann number decreases the average Nusselt number, with a more pronounced effect when the magnetic field is oriented horizontally. A higher permeability ratio reduces flow resistance and enhances convective heat transfer, but beyond $K > 10$, further increases in permeability have minimal impact on the heat transfer rate.

Key words: natural convection, anisotropic porous medium, nanofluid, numerical study, magnetic field.



1. Introduction

THE TERM NANOFUID, INTRODUCED FOR THE FIRST TIME by CHOI [1] refers to fluids in which nanometric particles are suspended in a base fluid. According to CHOI [1], the introduction of nanoparticles with higher thermal conductivity into the base fluid increased the thermal performance of the resultant nanofluid. The nanoparticle effect on natural convection was the object of many studies. For instance, HAMAD [2] studied natural convection around a horizontal flat surface in the presence of a magnetic field but found an inverse relationship between heat transfer and nanoparticle volume fraction, contrasting with other findings. This discrepancy highlights the need for further investigation into how nanoparticles interact with magnetic fields, especially under varying thermal and flow conditions. GÜRBÜZ-ÇALDAĞ and ÇELİK [3] used the radial basis function approximation to model Stokes flow in a lid-driven cavity under a homogeneous magnetic field with different inclination degrees and Hartmann values. The findings indicate that the inclination angle has a nonlinear effect on the stream function, although greater Hartmann numbers decrease its amplitude. The direction and strength of the magnetic field have an impact on vortex formation. The moving lid's velocity distribution is used to create smooth corner eddies. KAHVECI [4] investigated various types of nanoparticles within a differentially heated inclined enclosure. They were able to show that the heat transfer rate of the non-metallic particles is lower than that of the metallic nanoparticles. In addition, BILGEN [5] studied natural convection in an enclosure in which a thin fin was attached to the hot wall. He concluded that the Nusselt number increased in parallel with the Rayleigh number. However, the Nusselt number was a decreasing function of the relative thermal conductivity ratio as well as the fin length. GHASEMI *et al.* [6] conducted numerical investigations on natural convection phenomena in a square cavity filled with Al_2O_3 water under the influence of a horizontal magnetic field. The results indicate that the heat transfer rate decreases as the Hartmann number increases but increases as the Rayleigh number increases. Nevertheless, the values of the Hartmann and Rayleigh numbers are a measure of the improvement in heat transfer performance as the volume fraction of solids increases. The study by KHANAFER *et al.* [7] for natural convection heat transfer of a copper-water nanofluid in a square cavity, confirmed that the presence of nanoparticles in the fluid and their increased volume fraction enhances heat transfer for any given Grashof number, but their focus on a single type of nanofluid leaves open questions about how different nanofluids behave under comparable conditions.

In porous media, the extended Darcy–Brinkman model has been used to explore the impact of nanofluids on heat transfer efficiency, as seen in BOURANTAS *et al.* [8]. Alternative expressions were proposed to estimate the effective conduc-

tivity and the thermal expansion coefficient of the nanofluid, and their impacts on the heat transfer problem were examined. However, they did not fully consider how anisotropic properties influence these systems, which is crucial for understanding complex porous media applications. YADAV *et al.* [9] were interested in the effect of an internal heat source on the onset of Darcy–Brinkman convection in a porous layer saturated with a nanofluid. The study examined the influence of internal heat generation on the onset of Darcy–Brinkman convection in a nanofluid-saturated porous medium under various boundary conditions and combinations of physical parameters. They found that the internal heat source, the nanoparticle Rayleigh number, the modified diffusivity ratio and the Lewis number had a significant effect on the temperature and the volume fraction which deviate from linear to nonlinear trend, while increasing the Darcy number and porosity had an imperceptible effect on the temperature and volume fraction distributions.

Over the past few decades, there has been a considerable amount of research in which anisotropy has been explicitly taken into account, to provide a higher degree of accuracy and a deeper insight into the transport phenomena in porous media [10–13]. CHAND *et al.* [14] investigated the impact of variable gravity on thermal instability within an anisotropic porous horizontal layer saturated with a nanofluid. The results show that the decreasing gravity parameter has a stabilizing effect, while the increasing gravity parameter has a destabilizing effect on stationary convection but not fully explore how nanoparticle interactions change under these conditions. Likewise, the study by SAFI and BENISSAD [15] only addressed heat transfer in terms of specific anisotropic parameters, leaving out the interaction between permeability anisotropy and magnetic fields. A finite volume method has been employed to solve the coupling of the time-dependent Brinkman–Forchheimer and the double diffusion equations. The validity of the Brinkman–Forchheimer model for different combinations of the permeability ratio, thermal conductivity, the thermal Rayleigh number, the buoyancy ratio, an inclination angle and the Darcy number was the primary focus of the study. The effect of anisotropic properties on heat and mass transfer was demonstrated.

While natural convection in anisotropic porous media has been modeled, few studies have fully considered the combined effects of magnetic fields, anisotropy, and nanofluid properties. For instance, SHIVAKUMARA and DHANANJAYA [16] focused on internal heat generation, but their conclusions regarding nanoparticle influence remain incomplete, especially in complex geometric configurations. The study by AHMED and RASHAD [17] confirmed that increasing nanoparticle volume fraction improves heat transfer in anisotropic porous media but failed to address how varying permeability ratios and magnetic field inclinations might alter these results. Convective heat transfer in a Casson nanofluid saturated

in anisotropic porous enclosures of three types: shallow, square, and tall was studied by MAHESHWARI *et al.* [18]. They observed that in a shallow enclosure, heat transfer occurs more rapidly due to the onset of convection taking place earlier. Moreover, the study concludes that employing a Casson-based suspension of single-walled carbon nanotubes (SWCNTs) enhances heat transport and amplifies the magnitude of streamlines.

Recent research on natural convection heat transfer and fluid flow in nanofluids under magnetic fields has gained significant attention. BOURANTAS and LOUKOPOULOS [19] studied Al_2O_3 /water micropolar-nanofluids, demonstrating that both magnetic field strength and orientation significantly impact heat transfer. Finally, SHEIKHOESLAMI and ELLAHI [20] used a 3D mesoscopic model, showing that magnetic fields reduce convection while Nusselt numbers increase with Rayleigh numbers and nanoparticle concentration. EL-MAGHLANY *et al.* [21] analyzed CuO-water nanofluids in strong magnetic fields, revealing that heat transfer varied based on the field strength and the Rayleigh number. AL KALBANI *et al.* [22] explored natural convection in an inclined square enclosure, finding that increasing Rayleigh numbers and nanoparticle volume fractions enhanced heat transfer, while blade-shaped nanoparticles provided optimal results. ISLAM *et al.* [23] examined convective heat transfer in a semi-circular cavity with nanofluids under an inclined magnetic field. Their results showed that heat transfer improved with higher Rayleigh numbers, nanoparticle volume fractions, and magnetic field inclination, but decreased with higher Hartmann numbers. Cu- H_2O nanofluids performed best, with sinusoidal heating and the nanoparticle shape playing key roles.

The abovesummarized studies collectively demonstrate the complex interactions between magnetic fields, nanoparticle properties, and fluid flow in natural convection heat transfer, highlighting the importance of optimizing these parameters for enhanced thermal performance in engineering applications. The present study explores natural convection and heat transfer within a porous square enclosure filled with nanofluid, subjected to an external magnetic field at various inclinations and possessing anisotropic permeability properties. The motivation for this study is justified by the need to improve heat transfer efficiency in systems that rely on porous media, such as thermal insulation, geothermal energy extraction, and electronic cooling. While nanofluids and magnetic fields have been individually studied for their potential to enhance heat transfer, the combined effects of porous media anisotropy and an inclined magnetic field remain underexplored. The novelty of this study lies in considering the anisotropy of the porous medium combined with the use of a nanofluid, an aspect often neglected in current research on natural convection under the influence of a magnetic field. This approach is particularly important, as anisotropy can significantly impact the flow and heat transfer characteristics of nanofluids. By incorporating these

factors, the study offers a more accurate and comprehensive understanding of natural convection phenomena in various configurations, which is crucial for the design and optimization of nanofluid-based thermal systems.

2. Mathematical formulation

The configuration studied is shown in Fig. 1. It is a two-dimensional porous square enclosure of the length L and height H filled with $\text{Al}_2\text{O}_3/\text{water}$ nanofluid. The porous medium is anisotropic in permeability. The horizontal and vertical permeabilities of the porous medium are denoted by K_x and K_y , respectively. The anisotropy ratio is then defined as $K = K_x/K_y$. The left wall is maintained at a high temperature T_H , while the right wall is kept cold at T_C whereas the horizontal walls of the enclosure are adiabatic. The applied constant magnetic field with the strength B_0 is utilized on the left side of the cavity with angle γ along the positive horizontal direction. The nanofluid is assumed to be incompressible, Newtonian, and laminar. The thermophysical properties of the nanoparticles and the base liquid are presented in Table 1. A general model of Darcy–Brinkman–Forchheimer was used to account for the flow in the porous medium.

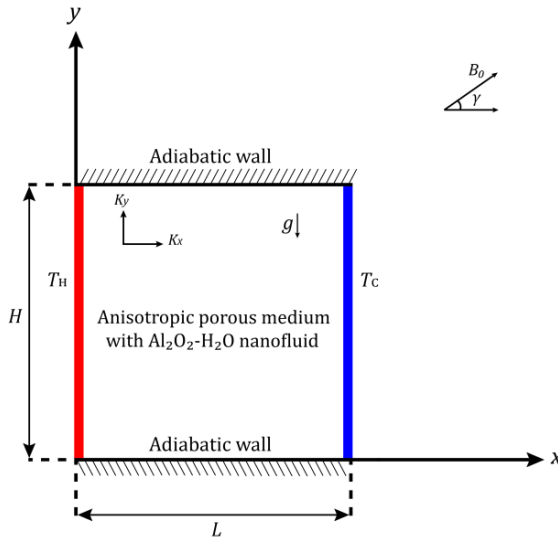


FIG. 1. Geometrical shape and boundary conditions.

The governing equations of the nanofluid flow and heat transfer under the Boussinesq approximation can be stated as follows [24, 25]. It should be noted that the present study considers the anisotropy of permeability in the porous medium while assuming isotropic thermal conductivity. However, in our previous

article [15], anisotropy was considered for both properties. As a result, the energy equation in [15] was expressed in an expanded form, incorrectly introducing a thermal conductivity tensor.

In the present study, it is therefore necessary to properly decompose the anisotropic terms in the following equations:

$$(2.1) \quad \frac{\partial u}{\partial x} + \frac{\partial v}{\partial y} = 0,$$

$$(2.2) \quad \frac{\rho_{nf}}{\varepsilon^2} \left(u \frac{\partial u}{\partial x} + v \frac{\partial u}{\partial y} \right) \\ = -\frac{\partial p}{\partial x} + \frac{\mu_{nf}}{\varepsilon} \left(\frac{\partial^2 u}{\partial x^2} + \frac{\partial^2 u}{\partial y^2} \right) - \left(\frac{\mu_{nf}}{K_x} \right) u - \frac{\rho_{nf} C_F \sqrt{u^2 + v^2}}{\sqrt{K_x}} u + f_{EM_x},$$

$$(2.3) \quad \frac{\rho_{nf}}{\varepsilon^2} \left(u \frac{\partial v}{\partial x} + v \frac{\partial v}{\partial y} \right) \\ = -\frac{\partial p}{\partial y} + \frac{\mu_{nf}}{\varepsilon} \left(\frac{\partial^2 v}{\partial x^2} + \frac{\partial^2 v}{\partial y^2} \right) - \left(\frac{\mu_{nf}}{K_y} \right) v - \frac{\rho_{nf} C_F \sqrt{u^2 + v^2}}{\sqrt{K_y}} v \\ + (\rho\beta)_{nf} g(T - T_C) + f_{EM_y},$$

$$(2.4) \quad (\rho c_p)_{nf} \left(u \frac{\partial T}{\partial x} + v \frac{\partial T}{\partial y} \right) = \frac{\partial}{\partial x} \left(k_m \frac{\partial T}{\partial x} \right) + \frac{\partial}{\partial y} \left(k_m \frac{\partial T}{\partial y} \right),$$

where ε is the porosity.

For a magnetic field at an orientation γ with respect to the horizontal plane, the components of the Lorentz force are expressed as follows

$$(2.5) \quad \begin{cases} f_{EM_x} = -\sigma_{nf}(B_0^2)(v \cos \gamma \sin \gamma - u \sin^2 \gamma), \\ f_{EM_y} = -\sigma_{nf}(B_0^2)(u \cos \gamma \sin \gamma - v \cos^2 \gamma). \end{cases}$$

Introducing the following dimensionless set:

$$(2.6) \quad (X, Y) = (x, y) \frac{1}{H}, \quad (U, V) = (u, v) \frac{H}{\alpha_f}, \quad P = p \frac{H^2}{\rho_{nf} \alpha_f^2}, \quad \theta = \frac{(T - T_C)}{(T_H - T_C)}.$$

This gives the following dimensionless equations:

$$(2.7) \quad \frac{\partial U}{\partial X} + \frac{\partial V}{\partial Y} = 0,$$

$$(2.8) \quad \frac{1}{\varepsilon^2} \left(U \frac{\partial U}{\partial X} + V \frac{\partial U}{\partial Y} \right) \\ = -\frac{\partial P}{\partial X} + \frac{\text{Pr}}{\varepsilon} \left(\frac{\rho_f}{\rho_{nf}} \right) \left(\frac{\mu_{nf}}{\mu_f} \right) \left(\frac{\partial^2 U}{\partial X^2} + \frac{\partial^2 U}{\partial Y^2} \right) \\ - \left(\frac{\rho_f}{\rho_{nf}} \right) \left(\frac{\mu_{nf}}{\mu_f} \right) \frac{\text{Pr}}{\text{Da} K} U - C_F \frac{\sqrt{U^2 + V^2}}{\sqrt{\text{Da} K}} U + F_{EM_x},$$

$$\begin{aligned}
 (2.9) \quad & \frac{1}{\varepsilon^2} \left(U \frac{\partial V}{\partial X} + V \frac{\partial V}{\partial Y} \right) \\
 & = -\frac{\partial P}{\partial Y} + \frac{\text{Pr}}{\varepsilon} \left(\frac{\rho_f}{\rho_{nf}} \right) \left(\frac{\mu_{nf}}{\mu_f} \right) \left(\frac{\partial^2 V}{\partial X^2} + \frac{\partial^2 V}{\partial Y^2} \right) - \left(\frac{\rho_f}{\rho_{nf}} \right) \left(\frac{\mu_{nf}}{\mu_f} \right) \frac{\text{Pr}}{\text{Da}} V \\
 & \quad - C_F \frac{\sqrt{U^2 + V^2}}{\sqrt{\text{Da}}} V + \left(\frac{(\rho\beta)_{nf}}{\rho_{nf}\beta_f} \right) \text{Ra Pr } \theta + F_{EM_Y}, \\
 (2.10) \quad & U \frac{\partial \theta}{\partial X} + V \frac{\partial \theta}{\partial Y} = \frac{(\rho c_p)_f}{(\rho c_p)_{nf}} \left[\frac{\partial}{\partial X} \left(\frac{k_m}{k_f} \frac{\partial \theta}{\partial X} \right) + \frac{\partial}{\partial Y} \left(\frac{k_m}{k_f} \frac{\partial \theta}{\partial Y} \right) \right].
 \end{aligned}$$

In this study, the thermal properties of the solid matrix and the nanofluid were assumed to be identical under the condition of local thermal equilibrium ($k_m = k_s = k_{nf}$), consistent with the assumptions used in several previous studies [26–30]. The energy equation for the porous medium is formulated as follows:

$$(2.11) \quad U \frac{\partial \theta}{\partial X} + V \frac{\partial \theta}{\partial Y} = \frac{\alpha_{nf}}{\alpha_f} \left(\frac{\partial^2 \theta}{\partial X^2} + \frac{\partial^2 \theta}{\partial Y^2} \right),$$

F_{EM_X} , F_{EM_Y} are respectively the dimensionless components of the Lorentz force along x and y , which are expressed as follows:

$$(2.12) \quad \begin{cases} F_{EM_X} = -\text{Pr} \left(\frac{\sigma_{nf}}{\sigma_f} \right) \left(\frac{\rho_f}{\rho_{nf}} \right) \text{Ha}^2 (V \cos \gamma \sin \gamma - U \sin^2 \gamma), \\ F_{EM_Y} = -\text{Pr} \left(\frac{\sigma_{nf}}{\sigma_f} \right) \left(\frac{\rho_f}{\rho_{nf}} \right) \text{Ha}^2 (U \cos \gamma \sin \gamma - V \cos^2 \gamma), \end{cases}$$

with C_F denotes the Forchheimer coefficient defined by:

$$(2.13) \quad C_F = \frac{1.75}{\sqrt{150} \varepsilon^{3/2}}.$$

The dimensionless parameters are defined as the Darcy number $\text{Da} = K_y/L^2$, the Prandtl number $\text{Pr} = \nu_f/\alpha_f$, the Rayleigh number $\text{Ra} = g\beta_f\Delta TH^3/(\alpha_f\nu_f)$, the Hartmann number $\text{Ha} = B_0L\sqrt{\sigma_f/\mu_f}$, and the permeability ratio $K = K_x/K_y$.

The non-dimensional boundary conditions associated with this problem are as follows:

$$(2.14) \quad \begin{cases} X = 0, & 0 \leq Y \leq 1 : U = V = 0, \theta = 1, \\ X = \frac{L}{H} = 1, & 0 \leq Y \leq 1 : U = V = 0, \theta = 0, \\ Y = 0, & 0 \leq X \leq 1 : U = V = 0, \frac{\partial \theta}{\partial Y} = 0, \\ Y = 1, & 0 \leq X \leq 1 : U = V = 0, \frac{\partial \theta}{\partial Y} = 0. \end{cases}$$

The nanofluid density ρ_{nf} , thermal expansion coefficient β_{nf} , heat capacity $(\rho c_p)_{nf}$, and thermal diffusivity α_{nf} are defined, respectively, as:

$$(2.15) \quad \rho_{nf} = (1 - \phi) \rho_f + \phi \rho_p,$$

$$(2.16) \quad (\rho\beta)_{nf} = (1 - \phi)(\rho\beta)_f + \phi(\rho\beta)_p,$$

$$(2.17) \quad (\rho c_p)_{nf} = (1 - \phi)(\rho c_p)_f + \phi(\rho c_p)_p,$$

$$(2.18) \quad \alpha_{nf} = k_{nf}/(\rho c_p)_{nf}.$$

The effective dynamic viscosity and thermal conductivity of the nanofluid are determined using the Brinkman model [31] for viscosity and the Maxwell model [32] for thermal conductivity, respectively, as follows:

$$(2.19) \quad \frac{\mu_{nf}}{\mu_f} = \frac{1}{(1 - \phi)^{2.5}},$$

$$(2.20) \quad \frac{k_{nf}}{k_f} = \frac{(k_p + 2k_f) - 2\phi(k_f - k_p)}{(k_p + 2k_f) + \phi(k_f - k_p)},$$

where ϕ and μ_f are respectively, the nanoparticle volume fraction and the fluid dynamic viscosity.

Also, the effective electrical conductivity for the used nanofluid is expressed as follows [33]:

$$(2.21) \quad \frac{\sigma_{nf}}{\sigma_f} = 1 + \frac{3(\sigma_p/\sigma_f - 1)\phi}{(\sigma_p/\sigma_f + 2) - (\sigma_p/\sigma_f - 1)\phi}.$$

TABLE 1. Thermo-physical properties of water and nanoparticles [34].

	ρ [kg/m ³]	c_p [J/kg · K]	k [W/m · K]	β [1/K]	σ [($\Omega \cdot \text{m}$) ⁻¹]
Water	997.1	4179	0.613	21×10^{-5}	0.05
Alumina (Al ₂ O ₃)	3970	765	40	0.85×10^{-5}	10^{-10}

The heat transfer coefficient in terms of the local Nusselt number is defined by:

$$(2.22) \quad \text{Nu}_{\text{loc}} = - \left(\frac{k_{nf}}{k_f} \right) \frac{\partial \theta}{\partial X}.$$

The average Nusselt number is defined as:

$$(2.23) \quad \text{Nu}_{\text{avg}} = \int_0^1 \text{Nu}_{\text{loc}} dY.$$

3. Numerical method and validation

The Darcy–Brinkman–Forchheimer and energy equations, along with their corresponding boundary conditions, were discretized using the finite volume method. The pressure-velocity coupling was handled using the SIMPLER numerical technique [35]. The governing equations were spatially discretized using second-order central finite difference schemes. Solving the system of algebraic equations directly is complicated, so we use the sweeping technique, a semi-iterative solving method. This method involves determining the values of the variable ϕ for each line of the study domain independently of the others, transforming the multi-dimensional algebraic system into a one-dimensional system by incorporating terms from other dimensions into the source term of the chosen dimension. The resulting system is represented by a Tri-Diagonal matrix, which can then be solved using the Line-by-line TriDiagonal Matrix Algorithm (LTDMA). The convergence criterion for this problem is defined as:

$$(3.1) \quad \left| \frac{\phi^n - \phi^{n-1}}{\phi^n} \right| < 10^{-5}.$$

In this case, ϕ denotes the various computed variables U , V , or θ , while n indicates the number of iterations.

The accuracy of the results and the computation time are closely related to the choice of grid. A uniform grid was used. To evaluate the effect of a grid size on the numerical solutions, four configurations were tested: 42×42 , 62×62 , 82×82 , and 132×132 nodes. When increasing the grid size from 82×82 to 132×132 nodes, a variation of less than 0.4% was observed in the calculated values (Table 2). After performing the numerical solution independence tests, the 82×82 node grid was selected, as it offers the best compromise between computation time and accuracy.

TABLE 2. Grid-independency results for Nusselt number and stream function when $\text{Ra} = 10^6$, $\gamma = 90^\circ$, $\text{Ha} = 50$, $\phi = 0.05$, $K = 1$ and $\text{Da} = 10^{-2}$.

Grid	52×52	62×62	82×82	132×132
Nu_{avg}	6.359	6.338	6.313	6.311
$ \psi _{\text{max}}$	13.522	13.406	13.304	13.301

To verify the reliability of the numerical simulations, the calculated average Nusselt number was compared with the numerical results of NI and BECKER-MANN [36], as shown in Table 3. Their study employed a control-volume formulation similar to the present method, with modifications for the momentum equations and anisotropic thermal conductivities in the energy equation. They

also optimized grid spacing iteratively to account for the boundary layer thickness. Based on the data from Table 3, a good match between the current findings and previously published results is observed. In addition, the present numerical results were validated by comparing them with data from natural convection studies in a differentially heated square cavity for $Ra = 10^5$ and $Pr = 0.7$. Figure 2 demonstrates that the results align very well with the experimental data from KRANE and JESSEE [37] and the numerical results of KHANAFER *et al.* [7], showing good agreement with very minor differences. It is to mention that KHANAFER *et al.* [7] employed the finite volume method, similar to the approach used in this study. However, their methodology for achieving a steady-state solution relied on a fake transient accelerator to speed up convergence. They solved the transient equations using the power-law method combined with an Alternating-Direction Implicit (ADI) scheme.

TABLE 3. Comparison of average Nusselt number with NI and BECKERMANN [36] for different K at $Ra = 10^3$ and $Pr = 0.71$.

K	Present work	NI and BECKERMANN [36]
10^{-3}	117.83	118.72
10^{-2}	80.57	80.34
10^{-1}	37.01	37.37
1	13.21	13.41
10	4.15	4.17
10^2	1.26	1.30
10^3	1.03	1.01

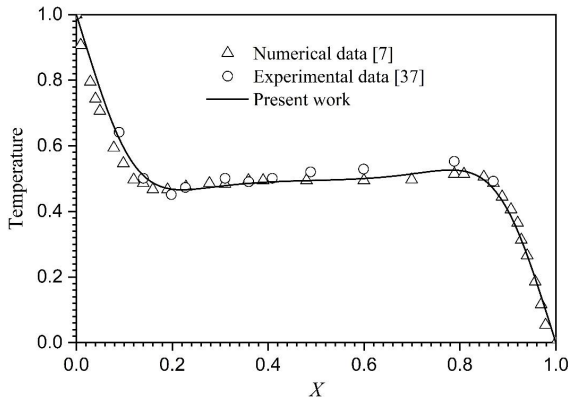


FIG. 2. Temperature distribution along the width of the cavity at $Y = 0.5$. Comparison of present work with other published data for $Ra = 10^5$ and $Pr = 0.7$.

A final validation of our computational code was conducted through a quantitative and qualitative comparison with the results of NGUYEN *et al.* [38]. It should be noted that the methodology employed in this work differs from that of [38], who used the finite element method (FEM) with the characteristic-based split (CBS) algorithm, implemented using the Galerkin technique. Table 4 presents a comparison of $|\psi|_{max}$ for the natural convection flow of a nanofluid in a porous cavity. These comparisons were made for $Ra = 10^7$, with porosity $\varepsilon = 0.4$ and volume fraction $\varphi = 0.025$, using the Brinkmann and Maxwell–Garnett models to calculate the viscosity and effective thermal conductivity of the nanofluid. As shown in Table 4 and Fig. 2, our results align almost perfectly

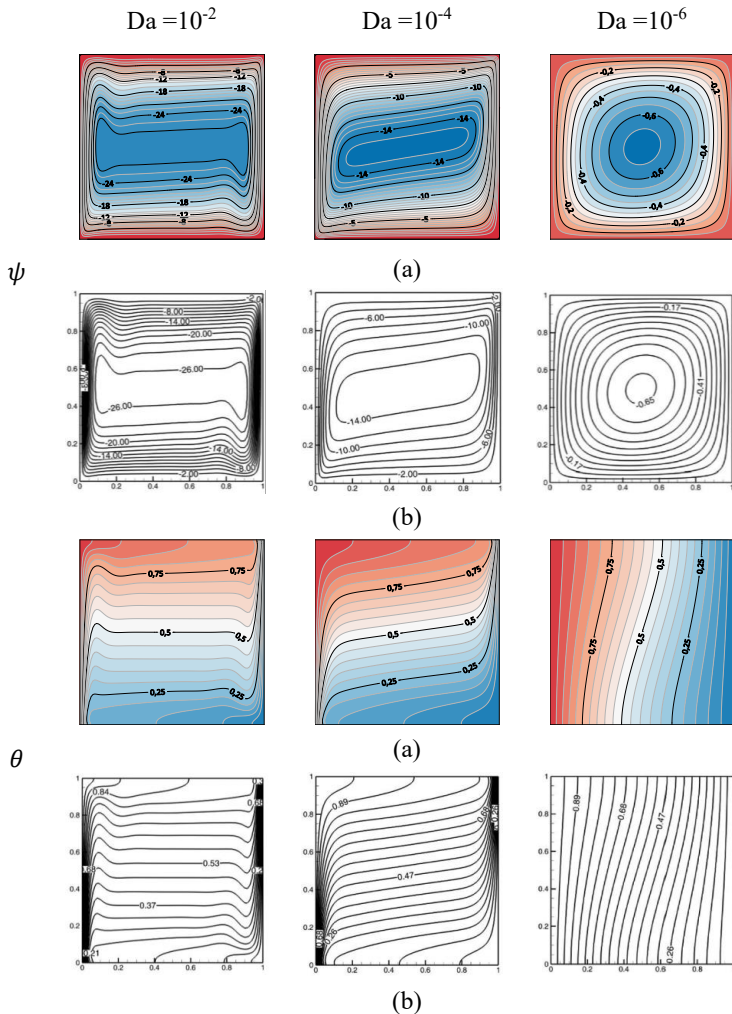


FIG. 3. Comparison of results with reference [38] for $Ra = 10^7$, $\varepsilon = 0.4$, and $\varphi = 0.025$.

TABLE 4. Comparison of the results with those of the literature reference [38].

	Da	$ \psi _{\max}$
NGUYEN <i>et al.</i> [38]	10^{-2}	27.515
Present result		27.038
NGUYEN <i>et al.</i> [38]	10^{-4}	14.975
Present result		14.711
NGUYEN <i>et al.</i> [38]	10^{-6}	0.665
Present result		0.671

with those from the literature, with a margin of error below 2%. This slight deviation underscores the reliability and precision of our simulation method.

4. Results and discussion

The results of the numerical simulation carried out to investigate the flow field, temperature distribution, and heat transfer in a square cavity filled with an anisotropic porous layer saturated by a nanofluid in the presence of a magnetic field are presented and discussed. The results present the effects of several parameters, such as nanoparticle volume fraction (φ) ranging from 0.01 to 0.09, the Darcy number (Da) between 10^{-2} to 10^{-4} , the Hartmann number (Ha) between 0 and 100, the Rayleigh number (Ra) between 10^3 and 10^6 , an inclination angle of magnetic field (γ) between 0° and 90° and the permeability ratio (K) between 10^{-1} and 10^3 , with a fixed porosity (ε) of 0.8, all of which are analyzed.

The contours of the streamlines and isotherms for different Darcy numbers and nanoparticle volume fractions are shown in Fig. 4 at $Ra = 10^5$, $K = 1$, $Ha = 50$ and $\gamma = 0^\circ$. The flow structure consists of a vertically elongated cell oriented in a clockwise direction, resulting from the presence of a horizontal magnetic field that generates a single component of the Lorentz force directed vertically. Generally, the presence of nanoparticles in the fluid causes the fluid flow structure to change, thereby influencing the thermal field. The increased permeability strengthens the flow inside the cavity, leading to a transition from conduction to convection. For the case $Da = 10^{-4}$, the influence of the volume fraction on the streamlines becomes more significant as a result of the increase in the effective dynamic viscosity. In this mode, the uniform distribution of isotherms is a result of the low permeability, indicating that heat transfer in the cavity is primarily driven by thermal conduction. With the increase of the Darcy number, the cells become bigger. Hence, for $Da = 10^{-2}$ and $Da = 10^{-3}$, the influence of volume fraction (φ) on the streamlines is quite minimal. Moreover, the Darcy number exerts a substantial impact on isotherms. Elevating it results in denser isotherms, consequently enhancing heat transfer.

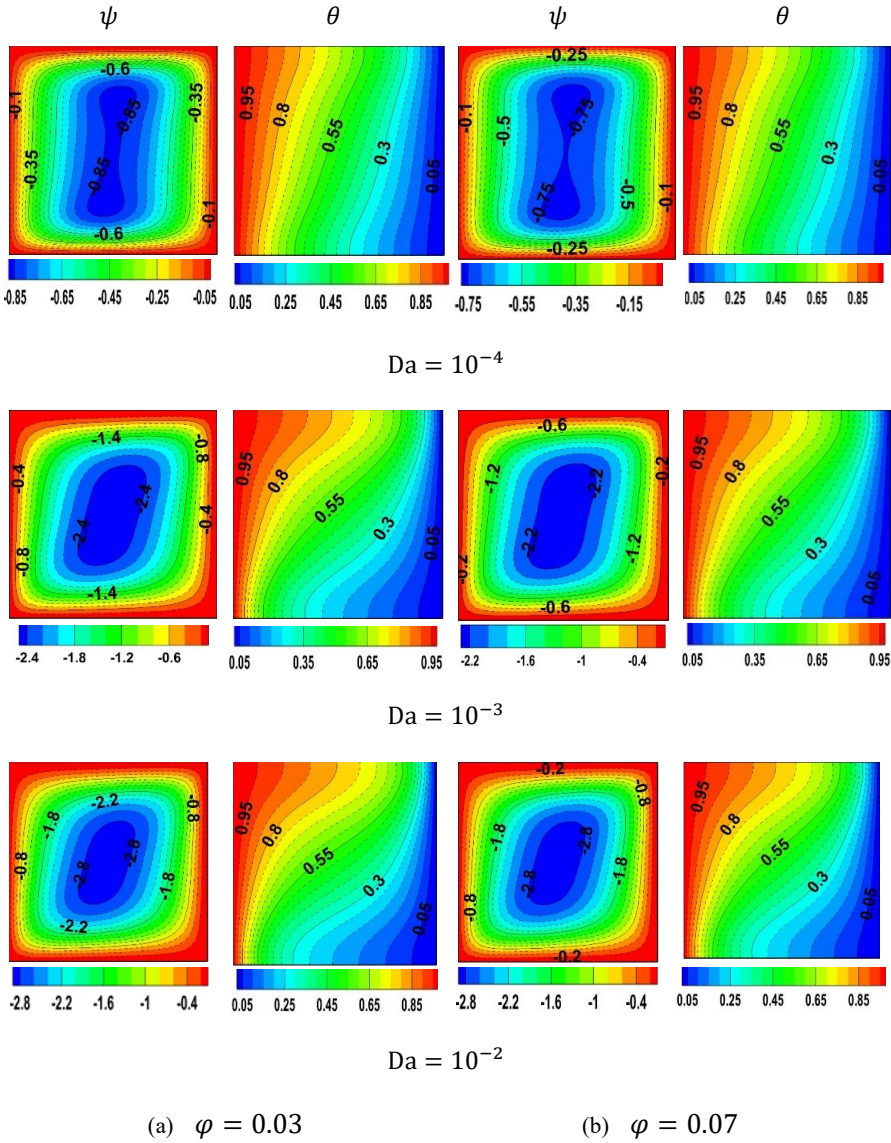


FIG. 4. Streamlines and isotherms for different φ and Da at $Ra = 10^5$, $\gamma = 0^\circ$, $Ha = 50$ and $K = 1$.

Figure 5 illustrates the effects of the magnetic field ($Ha = 0$ and 50) and its orientation (γ) on the streamlines and isotherms, for $Ra = 10^6$, $Da = 10^{-2}$, $\varphi = 0.07$ and $K = 1$. In the absence of a magnetic field, the flow is dominated by a large, clockwise convection cell. Under the effect of intensified natural convection, this cell deforms at the centre of the enclosure, generating two secondary cells within it. In the presence of the magnetic field, a weakening of the flow

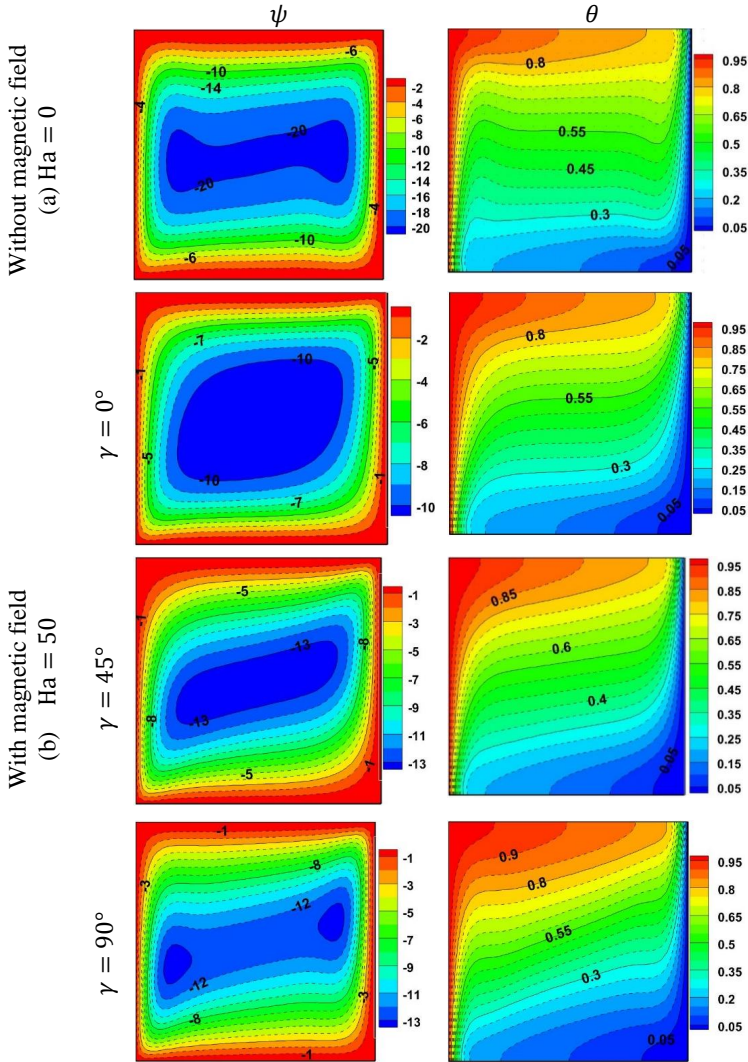


FIG. 5. Streamlines and isotherms for different Ha and γ at $Ra = 10^6$, $Da = 10^{-2}$, $\varphi = 0.07$ and $K = 1$.

intensity is observed, with a decrease in $|\psi|_{\max}$ from 20.758 ($Ha = 0$) to 13.432 ($Ha = 50$). However, three distinct patterns of the flow field appear at different orientations (0° , 45° , and 90°) due to the effect of the generated electromagnetic force.

Regarding the thermal field, significant deformation of the isotherms is observed near the isothermal walls at high Rayleigh numbers, indicating the predominance of the convective regime. As the Hartmann number (Ha) increases, conduction gradually becomes dominant over convection. The isotherms appear

less and less deformed, particularly near the isothermal walls. However, at the center of the enclosure, they remain parallel and gradually incline according to the magnetic field's inclination, shifting from a horizontal to a vertical orientation, unlike the case where $Ha = 0$, where they are aligned horizontally.

The effects of the permeability ratio (K) and the Darcy number (Da), with $Ra = 10^6$, $Ha = 50$, $\varphi = 0.05$ and $\gamma = 90^\circ$, on the flow fields and thermal structures are illustrated in Fig. 6. In an isotropic medium $K = 1$ under the influence of a vertical magnetic field, the flow is dominated by a large clockwise rotation cell when $Da = 10^{-4}$, due to the low permeability, which significantly restricts fluid motion. As permeability increases $Da = 10^{-2}$ the main cell deforms,

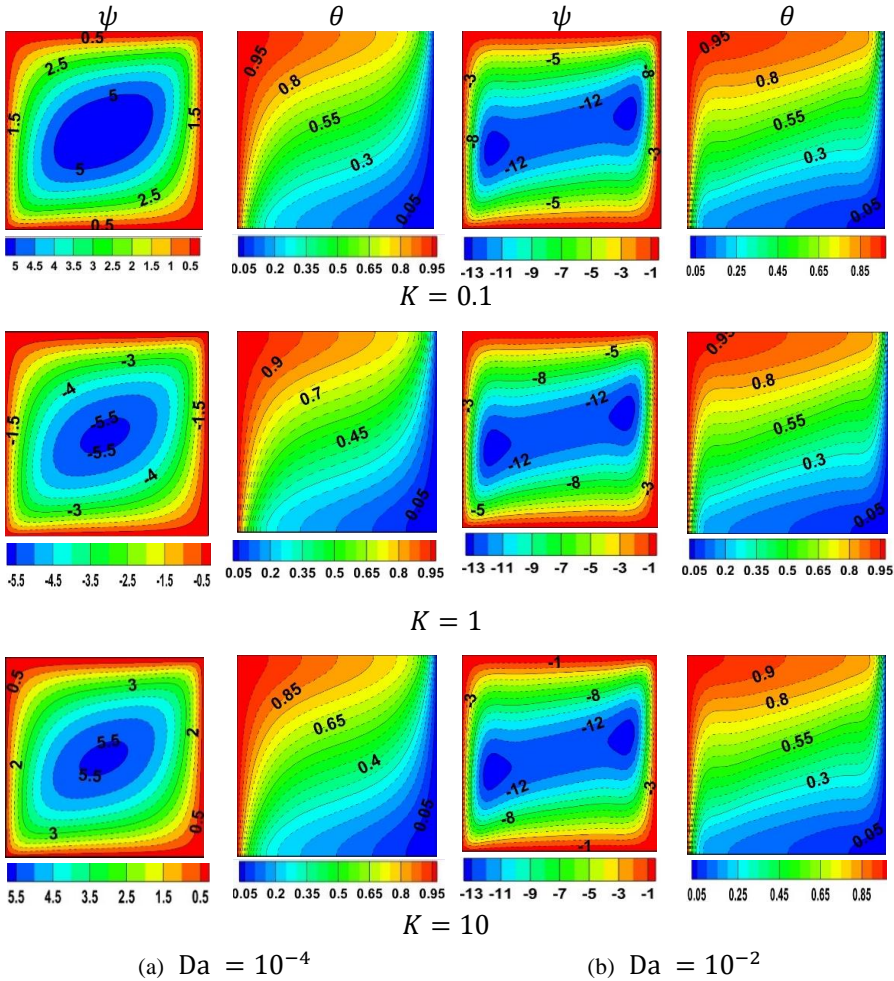


FIG. 6. Streamlines and isotherms for different Da and K at $Ra = 10^6$, $Ha = 50$, $\varphi = 0.05$ and $\gamma = 90^\circ$.

resulting in the generation of two inclined secondary cells. At low (Da) values, thermal conduction remains the primary heat transfer mechanism, leading to less deformation of the isotherms. With increasing (Da) the isotherms exhibit few significant changes; however, a progressive alignment is observed within the enclosure, characterized by a marked inclination and more pronounced temperature gradients near the isothermal walls. The impact of the permeability ratio (K) within the range of 0.1 to 10 indicates that horizontal permeability is less significant, contributing almost no resistance to flow. Consequently, the flow is primarily governed by buoyancy and controlled by the vertical resistance, which remains constant. In this context, the resistance is determined solely by the Darcy number (Da), suggesting that the flow structures and isotherm distribution are independent of the permeability ratio (K).

The influence of nanoparticle volume fraction (φ) and the Darcy number (Da) on the average Nusselt number for an anisotropic porous medium is shown in Fig. 7, at $Ra = 10^6$, $Ha = 50$, $\gamma = 90^\circ$ and $K = 0.1$. Firstly, it can be observed that the average Nusselt number increases as the Darcy number rises, due to convection becoming relatively significant. The addition of solid nanoparticles leads to two opposing effects: on one hand, a beneficial effect related to the presence of nanoparticles with high thermal conductivity, and on the other hand, a negative effect stemming from the increase in viscosity caused by these nanoparticles. For $Da = 10^{-2}$, increasing the concentration of nanoparticles leads to an increase in thermal conductivity and effective viscosity. Despite this rise in thermal conductivity, the adverse effect of viscosity makes the nanofluid more viscous. This

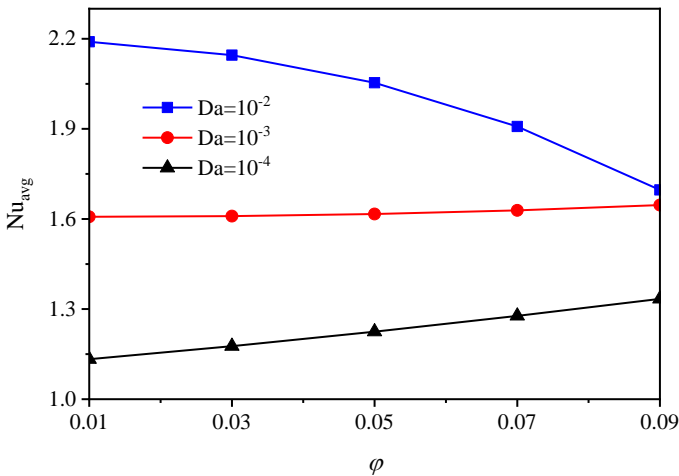


FIG. 7. Averaged Nusselt number Nu_{avg} for different φ and Da at $Ra = 10^6$, $\gamma = 90^\circ$, $Ha = 50$ and $K = 0.1$.

reduction in convection intensity consequently lowers the average Nusselt number. At low Darcy numbers ($Da = 10^{-3}$ and 10^{-4}), thermal conduction becomes the predominant mode, rendering the effect of effective viscosity negligible. Conversely, the effective thermal conductivity of the nanofluid contributes to an increase in the average Nusselt number.

Figure 8 presents the evolution of the average Nusselt number (Nu_{avg}) for different Hartmann numbers (Ha) and the permeability ratio (K) at $Ra = 10^6$, $\gamma = 90^\circ$, $Da = 10^{-2}$ and $\varphi = 0.05$. From Fig. 8, upon increasing the Hartmann number (Ha), the average Nusselt number decreases considerably and becomes less and less affected by (K) where the higher value of Nusselt number will be obtained at $Ha = 0$. In addition, the increase in the permeability ratio is also beneficial for heat transfer. This is due to reducing the dynamic boundary layer thickness.

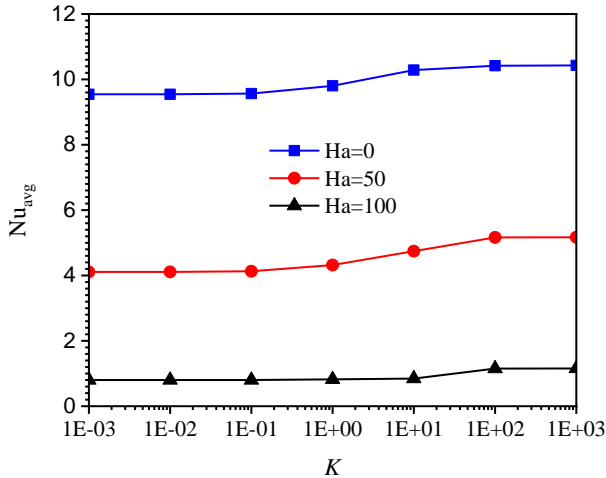


FIG. 8. Averaged Nusselt number Nu_{avg} for different K and Ha at $Ra = 10^6$, $\gamma = 90^\circ$, $Da = 10^{-2}$ and $\varphi = 0.05$.

However, the permeability ratio is increased from 10^2 to 10^3 , a convective regime occurs, resulting in a stronger convective flow. The transfer is intensive and tends to constant maximum values which are independent of (K) value.

Figure 9 shows the average Nusselt number (Nu_{avg}) versus the Hartmann number (Ha) for different angles of the magnetic field (γ) at $Da = 10^{-2}$, $\varphi = 0.07$, $Ra = 10^6$ and $K = 1$.

According to Fig. 9, the average Nusselt number decreases as the Hartmann number increases. This phenomenon is explained by the deceleration of the flow due to the electromagnetic force, which acts in opposition. The reduction in flow velocity leads to an increase in the thickness of the thermal boundary layer. This thickening reduces the temperature gradients at the isothermal

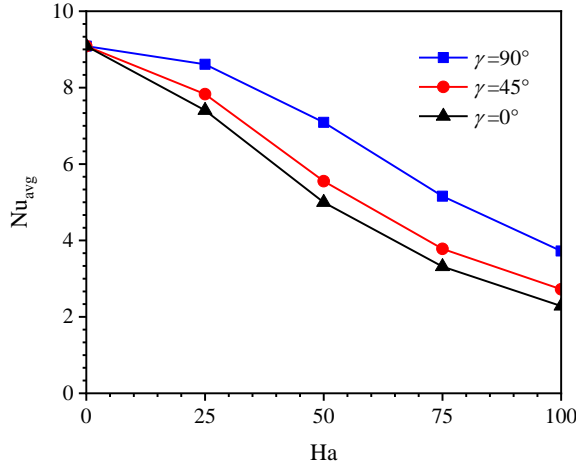


FIG. 9. Averaged Nusselt number Nu_{avg} for different Ha and γ at $Ra = 10^6$, $K = 1$, $Da = 10^{-2}$ and $\varphi = 0.05$.

surfaces, thereby lowering the average Nusselt number. The influence of the magnetic field orientation was also observed in the square enclosure, and it appears that the effect of the magnetic field is more pronounced in the horizontal direction. This is because the vertical Lorentz force generated significantly damps the flow, driven by buoyancy.

Figure 10 shows the variation of the average Nusselt number with the Rayleigh number at different values of the permeability ratio. It can be observed that the slopes of the Nusselt number versus Rayleigh number curves are quite

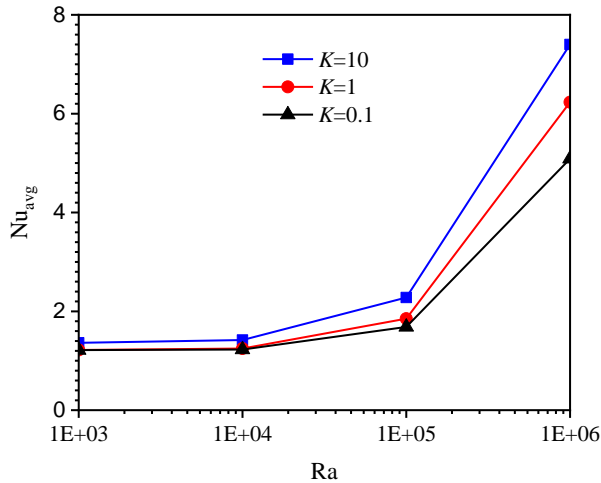


FIG. 10. Averaged Nusselt number Nu_{avg} for different Ra and K at $Ha = 50$, $Da = 10^{-2}$ and $\varphi = 0.05$.

similar for ranges of the permeability ratio. This increase is unimportant in the range with low values of the Rayleigh number, so the Nusselt number can be assumed to be independent of the Rayleigh number.

The impact of the permeability ratio K on the average Nusselt number is shown in Fig. 11 when $Ra = 10^6$, $Ha = 50$, $\varphi = 0.05$. The figure shows that the permeability ratio has a significant effect on heat transfer. As the permeability ratio decreases, the transfer becomes weaker. The decline in heat transfer is attributed to the flow weakening as (K) decreases. According to our choice of reference quantities, the decrease in (K) implies a fall in horizontal permeability, while vertical permeability remains constant and contained within the term (Da). With the permeability ratio (K) fixed, the transfer decreases along with the Darcy number. It is found that the average Nusselt number is at its maximum at the Darcy number $Da = 10^{-2}$.

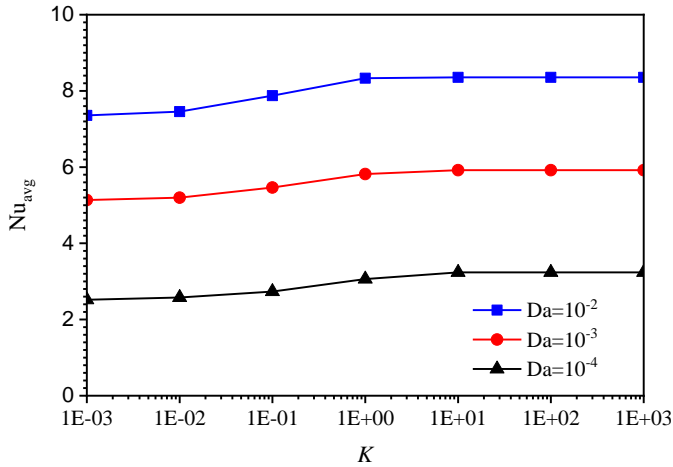


FIG. 11. Averaged Nusselt number Nu_{avg} for different K and Da at $Ha = 50$, $Ra = 10^6$, and $\varphi = 0.05$.

5. Conclusions

The present work is a numerical study of natural convection using the Darcy–Brinkman–Forchheimer model in a porous cavity saturated with a nanofluid. The porous medium was assumed to have anisotropic permeability. This study revealed the impact of various parameters on the flow field and heat transfer, specifically the volume fraction of nanoparticles, Darcy, Hartmann, and Rayleigh numbers, the angle of inclination of the magnetic field, and the permeability ratio. These factors significantly influence the evolution of the flow lines and isotherms, thereby modifying the heat transfer mechanisms.

The following conclusions can be drawn:

- The increase in Rayleigh and Darcy numbers favors the transition from a conduction-dominated regime to one dominated by convection, thereby improving the rate of heat transfer.
- The effect of the nanoparticle volume fraction (φ) is beneficial for the heat transfer rate in conduction-dominated flows but becomes unfavorable in a convection-dominated regime.
- Increasing the Hartmann number reduces the average Nusselt number, and this decrease is more pronounced when the magnetic field is oriented horizontally.
- Increasing the permeability ratio reduces flow resistance, thereby facilitating convective heat transfer.
- Once the permeability ratio $K > 10$, the heat transfer rate remains nearly constant, indicating that further increases in permeability no longer significantly enhance heat transfer.

References

1. S.U.S. CHOI, J.A. EASTMAN, *Enhancing thermal conductivity of fluids with nanoparticles*, (No. ANL/MSD/CP-84938; CONF-951135-29), Argonne National Lab. (ANL), Argonne, IL, United States of America, 1995.
2. M.A.A. HAMAD, *Analytical solution of natural convection flow of a nanofluid over a linearly stretching sheet in the presence of magnetic field*, International Communications in Heat and Mass Transfer, **38**, 4, 487–492, 2011, <https://doi.org/10.1016/j.icheatmasstransfer.2010.12.042>.
3. M. GÜRBÜZ-ÇALDAĞ, E. ÇELİK, *Stokes flow in lid-driven cavity under inclined magnetic field*, Archives of Mechanics, **74**, 6, 549–564, 2022, <https://doi.org/10.24423/aom.4013>.
4. K. KAHVECI, *Buoyancy driven heat transfer of nanofluids in a tilted enclosure*, Journal of Heat Transfer, **132**, 6, 062501, 2010, <https://doi.org/10.1115/1.4000744>.
5. E. BILGEN, *Natural Convection in Cavities with a thin fin on the hot wall*, International Journal of Heat and Mass Transfer, **48**, 17, 3493–3505, 2005, <https://doi.org/10.1016/j.ijheatmasstransfer.2005.03.016>.
6. B. GHASEMI, S.M. AMINOSADAT, A. RAISI, *Magnetic field effect on natural convection in a nanofluid-filled square enclosure*, International Journal of Thermal Sciences, **50**, 9, 1748–1756, 2011, <https://doi.org/10.1016/j.ijthermalsci.2011.04.010>.
7. K. KHANAFER, K. VAFAI, M. LIGHTSTONE, *Buoyancy-driven heat transfer enhancement in a two-dimensional enclosure utilizing nanofluids*, International Journal of Heat and Mass Transfer, **46**, 19, 3639–3653, 2003, [https://doi.org/10.1016/S0017-9310\(03\)00156-X](https://doi.org/10.1016/S0017-9310(03)00156-X).
8. G.C. BOURANTAS, E.D. SKOURAS, V.C. LOUKOPOULOS, V.N. BURGANOS, *Heat transfer and natural convection of nanofluids in porous media*, European Journal of Mechanics – B/Fluids, **43**, 45–56, 2014, <https://doi.org/10.1016/j.euromechflu.2013.06.013>.

9. D. YADAV, R. BHARGAVA, G.S. AGRAWAL, *Boundary and internal heat source effects on the onset of Darcy–Brinkman convection in a porous layer saturated by nanofluid*, International Journal of Thermal Sciences, **60**, 244–254, 2012, <https://doi.org/10.1016/j.ijthermalsci.2012.05.011>.
10. W.-J. CHANG, C.F. HSIAO, *Natural convection in a vertical cylinder filled with anisotropic porous media*, International Journal of Heat and Mass Transfer, **36**, 13, 3361–3367, 1993, [https://doi.org/10.1016/0017-9310\(93\)90017-Z](https://doi.org/10.1016/0017-9310(93)90017-Z).
11. P. NITHIARASU, K.S. SUJATHA, K. RAVINDRAN, T. SUNDARARAJAN, K.N. SEETHARAMU, *Non-Darcy natural convection in a hydrodynamically and thermally anisotropic porous medium*, Computer Methods in Applied Mechanics and Engineering, **188**, 1-3, 413–430, 2000, [https://doi.org/10.1016/S0045-7825\(99\)00163-2](https://doi.org/10.1016/S0045-7825(99)00163-2).
12. D.J. KRISHNA, T. BASAK, S.K. DAS, *Natural convection in a heat generating hydrodynamically and thermally anisotropic non-Darcy porous medium*, International Journal of Heat and Mass Transfer, **51**, 19-20, 4691–4703, 2008, <https://doi.org/10.1016/j.ijheatmasstransfer.2008.02.019>.
13. M.A. ABDELRAHEEM, S.E. AHMED, *An incompressible smoothed particle hydrodynamics method for natural/mixed convection in a non-Darcy anisotropic porous medium*, International Journal of Heat and Mass Transfer, **77**, 1155–1168, 2014, <https://doi.org/10.1016/j.ijheatmasstransfer.2014.06.044>.
14. R. CHAND, G.C. RANA, S. KUMAR, *Variable gravity effects on thermal instability of nanofluid in anisotropic porous medium*, International Journal of Applied Mechanics and Engineering, **18**, 3, 631–642, 2013, <https://doi.org/10.2478/ijame-2013-0038>.
15. S. SAFI, S. BENISSAAD, *Double-diffusive convection in an anisotropic porous layer using the Darcy–Brinkman–Forchheimer formulation*, Archives of Mechanics, **70**, 1, 89–102, 2018.
16. I.S. SHIVAKUMARA, M. DHANANJAYA, *Penetrative Brinkman convection in an anisotropic porous layer saturated by a nanofluid*, Ain Shams Engineering Journal, **6**, 2, 703–713, 2015, <https://doi.org/10.1016/j.asej.2014.12.005>.
17. S.E. AHMED, A.M. RASHAD, *Natural convection of micropolar nanofluids in a rectangular enclosure saturated with anisotropic porous media*, Journal Porous Media, **19**, 8, 737–750, 2016, <https://doi.org/10.1615/JPorMedia.v19.i8.60>.
18. S. MAHESHWARI, Y.D. SHARMA, O.P. YADAV, *Study of Heat Transfer in Anisotropic Porous Enclosures Saturated with Casson Fluid*, Journal of Porous Media, **26**, 10, 85–107, 2023, <https://doi.org/10.1615/JPorMedia.2023044926>.
19. G.C. BOURANTAS, V.C. LOUKOPOULOS, *MHD natural-convection flow in an inclined square enclosure filled with a micropolar-nanofluid*, International Journal of Heat and Mass Transfer, **79**, 930–944, 2014, <https://doi.org/10.1016/j.ijheatmasstransfer.2014.08.075>.
20. M. SHEIKHOESLAMI, R. ELLAHI, *Three dimensional mesoscopic simulation of magnetic field effect on natural convection of nanofluid*, International Journal of Heat and Mass Transfer, **89**, 779–808, 2015, <https://doi.org/10.1016/j.ijheatmasstransfer.2015.05.110>.
21. W.M. EL-MAGHLANY, M.M. ABO ELAZM, M. ELHELW, S. BAYOUMI, *The constraints on nanoparticles addition in natural convection heat transfer at highly magnetic field*, Journal of Thermophysics and Heat Transfer, **32**, 1, 2017, <https://doi.org/10.2514/1.T5183>.
22. K.S. AL KALBANI, M.M. RAHMAN, M.S. ALAM, N. AL-SALTI, A.I. ELTAYAB, *Buoyancy induced heat transfer flow inside a tilted square enclosure filled with nanofluids in the*

- presence of oriented magnetic field*, Heat Transfer Engineering, **39**, 6, 511–525, 2018, <https://doi.org/10.1080/01457632.2017.1320164>.
23. T. ISLAM, M.D. FAYZ-AL-ASAD, M.A. KHATUN, N. PARVEEN, H. AHMAD, S. ASKAR, *Natural convection heat transport performance of nanofluids under the influence of inclined magnetic field*, Results in Physics, **5**, 8, 107365, 2024, <https://doi.org/10.1016/j.rinp.2024.107365>.
 24. D.J. KRISHNA, T. BASAK, S.K. DAS, *Natural convection in a non-Darcy anisotropic porous cavity with a finite heat source at the bottom wall*, International Journal of Thermal Sciences, **48**, 7, 1279–1293, 2009, <https://doi.org/10.1016/j.ijthermalsci.2008.11.022>.
 25. A.M. ALY, S.E. AHMED, *An incompressible smoothed particle hydrodynamics method for natural/mixed convection in a non-Darcy anisotropic porous medium*, International Journal of Heat and Mass Transfer, **77**, 1155–1168, 2014, <https://doi.org/10.1016/j.ijheatmasstransfer.2014.06.044>.
 26. G. LAURIAT, V. PRASAD, *Non-Darcian effects on natural convection in a vertical porous enclosure*, International Journal of Heat and Mass Transfer, **32**, 11, 2135–2148, 1989, [https://doi.org/10.1016/0017-9310\(89\)90120-8](https://doi.org/10.1016/0017-9310(89)90120-8).
 27. P. NITHIARASU, K.N. SEETHARAMU, T. SUNDARARAJAN, *Natural convective heat transfer in a fluid saturated variable porosity medium*, International Journal of Heat and Mass Transfer, **40**, 16, 3955–3967, 1997, [https://doi.org/10.1016/S0017-9310\(97\)00008-2](https://doi.org/10.1016/S0017-9310(97)00008-2).
 28. X.B. CHEN, P. YU, S.H. WINOTO, H.T. LOW, *Free convection in a porous wavy cavity based on the Darcy–Brinkman–Forchheimer extended model*, Numerical Heat Transfer, Part A, **52**, 37–397, 2007, <https://doi.org/10.1080/10407780701301595>.
 29. M. KUMARI, G. NATH, *Unsteady natural convection from a horizontal annulus filled with a porous medium*, International Journal of Heat and Mass Transfer, **51**, 19–20, 5001–5007, 2008, <https://doi.org/10.1016/j.ijheatmasstransfer.2008.01.030>.
 30. G.H.R. KEFAYATI, *Heat transfer and entropy generation of natural convection on non-Newtonian nanofluids in a porous cavity*, Powder Technology, **299**, 127–149, 2016, <https://doi.org/10.1016/j.powtec.2016.05.032>.
 31. H.C. BRINKMAN, *The viscosity of concentrated suspensions and solutions*, The Journal of Chemical Physics, **20**, 4, 571–581, 1952.
 32. J.C. MAXWELL GARNETT, *Colours in metal glasses and in metallic films*, The Philosophical Transactions of the Royal Society A, **203**, 385–420, 1904.
 33. J.C. MAXWELL, *A Treatise on Electricity and Magnetism*, 2nd ed., Oxford University Press, Cambridge, 1904.
 34. F. BERRAHIL, A. FILALI, C. ABID, S. BENISSAAD, R. BESSAÏH, O. MATAR, *Numerical investigation on natural convection of Al₂O₃/water nanofluid with variable properties in an annular enclosure under magnetic field*, International Communications in Heat and Mass Transfer, **126**, 105408, 2021, <https://doi.org/10.1016/j.icheatmasstransfer.2021.105408>.
 35. S.V. PATANKAR, *Numerical Heat Transfer and Fluid Flow*, McGraw-Hill, New York, 1980.
 36. J. NI, C. BECKERMANN, *Natural convection in a vertical enclosure filled with anisotropic porous media*, Journal of Heat Transfer, **113**, 1033–1037, 1991.
 37. R.J. KRANE, J. JESSEE, *Some detailed field measurements for a natural convection flow in a vertical square enclosure*, [in:] 1st ASME-JSME Thermal Engineering Joint Conference, 1983.

-
38. M.T. NGUYEN, A.M. ALY, S.-W. LEE, *Natural convection in a non-Darcy porous cavity filled with Cu–Water nanofluid using the characteristic-based split procedure in finite-element method*, Numerical Heat Transfer, Part A: Applications, **67**, 2, 224–247, 2014, <https://doi.org/10.1080/10407782.2014.923225>.

Received June 28, 2024, revised version January 30, 2025.

Published online April 2, 2025.
